

## Hard Carbon Derived from Coal Tar Pitch for Use as the Anode Material in Lithium Ion Batteries

Zhihua Guo<sup>1</sup>, Chengyang Wang<sup>1,\*</sup>, Mingming Chen<sup>1</sup>, Mingwei Li<sup>2</sup>

<sup>1</sup> Key Laboratory for Green Chemical Technology of Ministry of Education, School of Chemical Engineering and Technology, Tianjin University, Tianjin 300072, China

<sup>2</sup> School of Science, Tianjin University, Tianjin 300072, China

\*E-mail: [cywang@tju.edu.cn](mailto:cywang@tju.edu.cn)

Received: 29 November 2012 / Accepted: 30 December 2012 / Published: 1 February 2013

---

A hard carbon (HC) material was prepared from isotropic coal tar pitch (CTP) by a simple oxidation-carbonization two-step method. Structural analysis showed that the CTP-HC material was a kind of microporous carbon, which was poorly crystallized and contains some graphite-like micro-crystallites. The CTP-HC was investigated as the anode material for lithium ion battery and the reversible capacity of CTP-HC was 576 mAh g<sup>-1</sup> with a corresponding coulombic efficiency of 69.5%. After 30 cycles, the reversible capacity of 350.8 mAh g<sup>-1</sup> was still achieved. Moreover, the CTP-HC delivered a high reversible capacity of 145 mAh g<sup>-1</sup> at a charging rate of 5C (1860 mAh g<sup>-1</sup>), which is much better than that (36 mAh g<sup>-1</sup>) of commercial graphitized mesocarbon microbeads (g-MCMB). The excellent electrochemical performance is attributed to the high porosity and the graphite-like micro-crystallites.

---

**Keywords:** Coal tar pitch; Carbon material; Microstructure; Lithium ion battery; Electrochemical performance

### 1. INTRODUCTION

Lithium ion batteries have been widely used in portable electronic devices, due to their high energy densities and long cycle lives [1, 2]. In recent years, the electrochemical performance of lithium ion batteries has been considerably enhanced. However, further improvement of reversible capacity, rate capability and cycle stability is still highly desirable for expanding its application in large-scale energy storage devices. The key for this further enhancement is to develop excellent performance electrode materials.

Various anode materials such as lithium alloys, carbonaceous materials, metal oxides, chalcogenides, and polymers have been proposed. Of all the materials investigated, carbonaceous materials have received considerable attention for its low cost, chemical and thermal stability,

environmental friendliness, and abundance in source. Currently, graphite is the most commonly used anode material because of its low electrode potential relative to lithium metal, low cost, high stability, and high initial coulombic efficiency. Nevertheless, low theoretical capacity ( $372 \text{ mAh g}^{-1}$ ) and slow diffusion coefficient of lithium ions through highly crystallized graphite restrict its applications in high-power devices [3]. Thus, researchers have turned to develop new carbon materials with different morphologies and structures.

Hard carbon material initially drew attention when Kureha firstly commercialized CARBOTRON P in 1991. The unique “house of cards” structure [4] of hard carbon enabled it display larger capacity and better rate performance than graphite. Since then, many efforts have been made to investigate and optimize of this carbon material. One effective method to improve the electrochemical performance of hard carbon material is reducing its particle size. Nanostructured hard carbon material can not only shorten the transport length of lithium ions but also offer tremendous electrode/electrolyte interface facilitating the charge-transfer reaction, which ensure excellent rate capability. Various nanostructured hard carbons, such as carbon nanobeads [5], carbon nanocages [6], hollow carbon nanospheres [7], and carbon nanofibers [8] have been reported. However, considerable irreversible capacity and low coulombic efficiency in initial cycle were found simultaneously with large specific surface area. Another method is preparing hard carbon from different precursors to improve its electrochemical performance. Numerous precursors including polymers, fossil fuels, and biomasses have been investigated. Among them, coal tar pitch became a promising candidate for its low cost, abundance, and relatively high carbon content. Mochida et al. [9] have investigated the insertion mechanism of hard carbon prepared from synthetic isotropic pitches. Fujimoto et al. [10] have studied the oxidation effect of coal tar pitch on the carbon structure and its anodic performance for lithium ion battery. They found that smaller crystal, lower staking or more content in the precursors ensures hard carbon large capacity. However, the microstructure of pitch-based hard carbon, and the relationship between the structure of hard carbon and its anodic performances have not been clarified.

In this work, an isotropic coal tar pitch with a high softening point was chosen as the precursor to prepare hard carbon by a simple two-step solid phase oxidation and carbonization method. The microstructure of the prepared coal tar pitch-based hard carbon and its anodic performance was characterized and investigated. It exhibits a large reversible capacity and high initial coulombic efficiency, an excellent rate performance, and good cycle performance. The excellent electrochemical performance is attributed to the high porosity and the existence of graphite-like micro-crystallites.

## 2. EXPERIMENTAL

### 2.1 Material preparation and structure characterization

An isotropic coal tar pitch with a high softening point around  $270 \text{ }^\circ\text{C}$  was used as the starting material, and was prepared according to the procedure described in our previous report [11]. The isotropic coal tar pitch was first pulverized to ca.  $20 \text{ }\mu\text{m}$  and then oxidized in a programmable tube furnace under a flow of air at  $330 \text{ }^\circ\text{C}$  (heating rate:  $0.5 \text{ }^\circ\text{C min}^{-1}$ ) for 2 h to convert the pitch to

thermosetting pitch. Coal tar pitch-based hard carbon (CTP-HC) was then easily obtained by carbonizing the stabilized pitch at 800 °C (heating rate: 2 °C min<sup>-1</sup>) for 2 h under a flow of N<sub>2</sub>. A commercial graphitized mesocarbon microbead (g-MCMB) provided by Tianjin Tiecheng Battery Material Co., Ltd with a diameter of the 10 μm was used for comparison.

Nitrogen adsorption-desorption measurements were conducted on a Micromeritics ASAP 2020 system. The morphologies of the samples were observed with a field emission scanning electron microscope (FESEM, Nano 430). The crystallinity was characterized by X-ray diffraction (XRD) on a D/Max 2500 X-ray diffractometer with Cu K $\alpha$  radiation (40 KV, 200 mA,  $\lambda = 1.54056 \text{ \AA}$ ). Raman spectrum was collected with a Renishaw inVia reflex Raman microscope using the 532 nm line of the Ar-ion laser as the excitation source. Detailed structural image was acquired with a high-resolution transmission electron microscope (HETEM, Philips Tecnai G2 F20) Elemental analysis was carried out on a CHN elemental analyzer (Vario Micro cube, Elementar).

## 2.2. Electrode, battery preparation and electrochemical measurement

The obtained carbon material, polyvinylidene fluoride (PVDF) and carbon black were mixed (88:7:5 by weight) in an agate mortar and then dispersed in N-methyl-2-pyrrolidone (NMP) to form a slurry. The working electrodes were fabricated by spreading the slurry onto copper foil and then dried at 120 °C for 12 h under vacuum. Lithium sheets were used as the counter-electrodes. The cells were assembled in a glove box filled with argon. The electrolyte was 1 M LiPF<sub>6</sub> in a mixture of ethylene carbonate (EC) and diethyl carbonate (DEC) (1:1 by volume). The assembled cells were galvanostatically charged and discharged in the voltage range of 0-2.0 V at different rates from 0.1 to 5 C using a multichannel Land Battery Test System. The cyclic voltammetry (CV) was performed on a Parstat 2273 potentiostat/galvanostat analyzer (Princeton Applied Research & AMTECT Company) at a scanning rate of 0.05 mV s<sup>-1</sup>.

## 3. RESULTS AND DISCUSSION

### 3.1 Morphology and structure characterization

The FESEM of the CTP-HC is presented in Fig. 1a. The prepared powders consist of sharp-edged particles and stacks together. The sizes of these particles range from 1 to 10 μm. The crystal structure of CTP-HC is investigated by Raman spectroscopy (Fig. 1b) and XRD (Fig. 1c). As shown in Fig. 1b, the Raman spectrum of CTP-HC exhibits two peaks at 1333 and 1598 cm<sup>-1</sup>, which respectively correspond to the D-band and G-band of polycrystalline carbon. The D-band at 1333 cm<sup>-1</sup> is attributed to defects, curved sheets and dangling bonds in the carbon structures, whereas the G-band at 1598 cm<sup>-1</sup> corresponds to the E<sub>2g</sub> mode of graphite [12]. Generally, the relative intensity of the D-band to that of the G-band ( $I_D/I_G$ ) represents the degree of disorder in the graphite structure [13]. For the CTP-HC, the  $I_D/I_G$  is 0.96, indicating a relatively low degree of graphitization of the CTP-HC. The XRD pattern of CTP-HC is presented in Fig. 1c, Two broad peaks around 23.2° and 43.5° are

observed, corresponding to the (002) diffraction and the (100) or (101) diffraction peaks of graphite [14]. The d-spacing between the (002) plane of CTP-HC is 0.383 nm calculated by Scherrer formula, which is larger than that of graphite. The two broad peaks and the large d-spacing indicate that the CTP-HC is an amorphous carbon containing small domains of coherent and parallelly stacked graphene sheets [15]. Furthermore, the peak tail that appears in the low Bragg region suggests the existence of micropores in the CTP-HC [16]. The crystalline features and the pore structures were further observed by TEM. As seen in Fig. 1d, the CTP-HC is poorly crystallized and contains some contacted graphite-like micro-crystallites, which are constructed by several short-range parallel graphene sheets (as shown in Fig. 1d). The distance between paralleled graphene sheets is measured to be 0.379 nm, and the value is in good agreement with the XRD results. Meanwhile, the graphite-like micro-crystallites are embedded by disordered graphene sheets. Such a disordered structure can lead to the formation of micropores and may act as “reservoirs” for lithium ion storage [17].

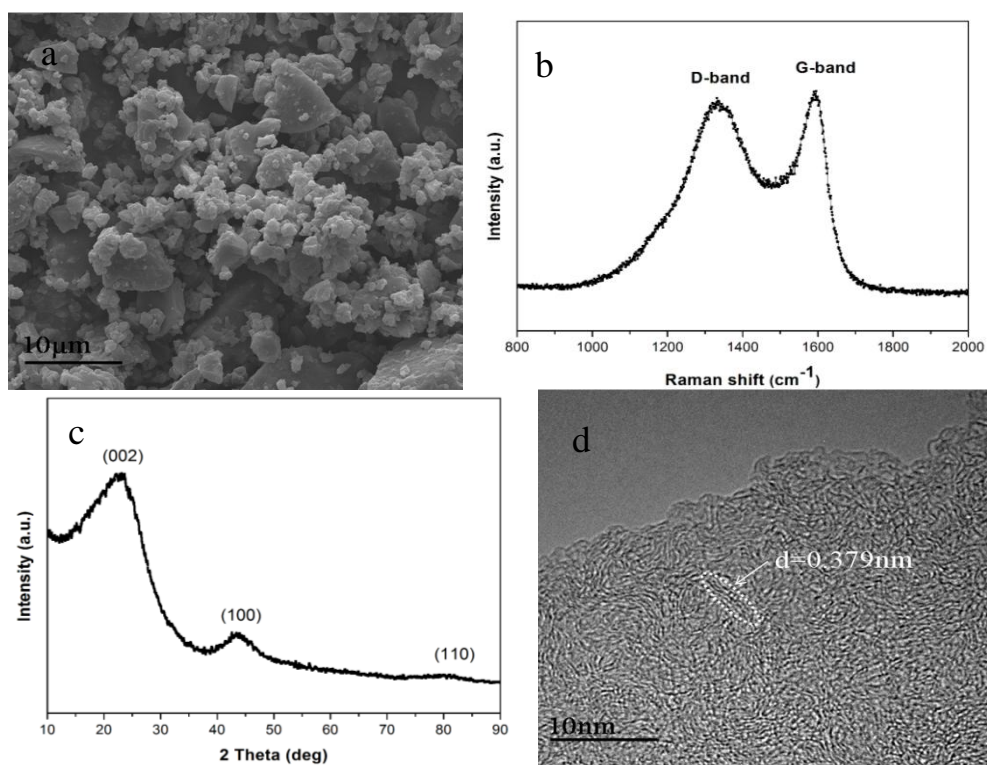


**Figure 1.** (a) FESEM image, (b) Raman spectrum, (c) XRD pattern, and (d) TEM image of CTP-HC.

The nitrogen adsorption-desorption was measured to further examine the porous structure of CTP-HC (Fig. 2). It is seen that the isotherm give rise to a type I curve. The Brunauer-Emmett-Teller (BET) surface area is around  $187 \text{ m}^2 \text{ g}^{-1}$  and the micropore volume is  $0.1 \text{ cm}^3 \text{ g}^{-1}$ . The pore size distribution is shown in the inset of Fig. 2. It can be seen that CTP-HC possess two micropores peaked at 0.73 and 1.35 nm, indicating that the CTP-HC is a microporous material. And the result is consistent to the XRD results and the observation of TEM. The elemental analysis indicate the content of C in the miroporous CTP-HC is 85.0 wt.% with additional 1.6 wt.% H and 1.3 wt.% N. The presence of heteroatoms can enhance reactivity and electrical conductivity of the material [18].

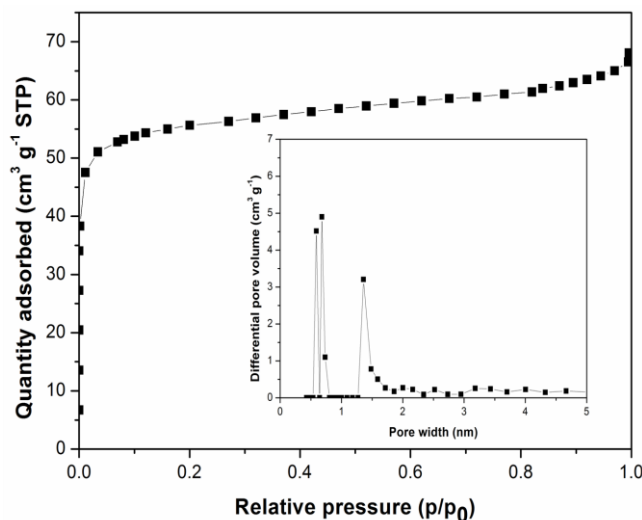


**Figure 2.** Nitrogen adsorption isotherm and pore size distribution (inset) of CTP-HC.

### 3.2 Electrochemical characterization

The as-prepared CTP-HC was investigated as the anode material for lithium ion battery and its electrochemical performance is presented in Fig 3. As shown in Figure 3a, the CTP-HC shows typical cyclic voltammetry (CV) curves of hard carbon. An apparent irreversible region can be seen from 0 to 1.25 V in the first cycle, which is originated from the electrolyte decomposition on the electrode/electrolyte surface and irreversible lithium insertion into potentially unique positions, such as cavities or sites in the vicinity of residual hydrogen atoms in the carbon material [19].

Figure 3b shows the first two charge/discharge curves of the prepared hard carbon at a current density of 0.1 C (37.2 mA g<sup>-1</sup>). In the first cycle, the CTP-HC has a charge capacity of 829 mAh g<sup>-1</sup> and a discharge capacity of 576 mAh g<sup>-1</sup>, with a corresponding coulombic efficiency of 69.5%. No obvious plateau or staging phenomenon was observed in the first charge curve, indicating a low degree of graphitization in the CTP-HC. The slope between 1 and 0.7 V is ascribed to the formation of a solid electrolyte interface [20]. The discharge curves show three different potential regions which may be attributed to different mechanisms. The region from 0 to 0.12 V corresponds to the deintercalation of lithium ions from the micropores in the randomly oriented stacks of small constituent molecules. The region from 0.12 to 0.8 V is ascribed to the deintercalation of lithium ions from the disordered graphene layers and the region above 0.8 V corresponds to the deintercalation of lithium from a variety of edge sites or from the H-/O-containing functional groups in the graphene layer [21].

Figure 3c illustrates the cycle performance of the CTP-HC. The coulombic efficiency in the first cycle is 69.5% and goes up to above 94% from the second cycle in all cases. After 30 cycles, a reversible capacity of 350.8 mAh g<sup>-1</sup> is still achieved.

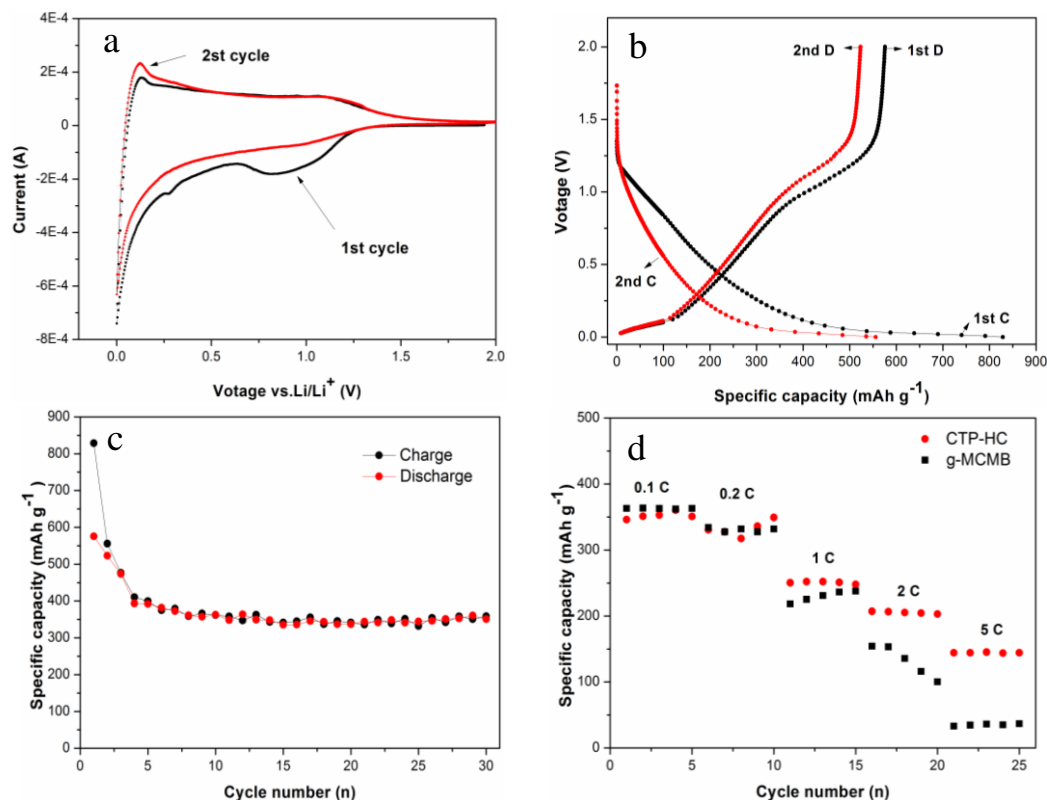


**Figure 3.** Electrochemical performances of CTP-HC: (a) cyclic voltammetry at a scan rate of  $0.05 \text{ mV s}^{-1}$ , (b) charge/discharge curves at a current density of  $37.2 \text{ mA g}^{-1}$ , (c) cycle performance at a current density of  $37.2 \text{ mA g}^{-1}$ , and (d) rate performance compared with g-MCMB.

Figure 3d shows the comparative rate performance of CTP-HC and g-MCMB. The cells were first cycled at 0.1C, followed by cycling at current densities increasing stepwise to 5C. When cycled at 0.1 or 0.2 C, the reversible capacity of the CTP-HC is comparable to that of the g-MCMB. However, when the charging rate is increased to 2 C ( $744 \text{ mA g}^{-1}$ ) or 5 C ( $1860 \text{ mA g}^{-1}$ ), the reversible capacity of CTP-HC is respectively 207 or  $145 \text{ mAh g}^{-1}$ . Whereas the g-MCMB only 135 or  $36 \text{ mAh g}^{-1}$  respectively, indicating the CTP-HC exhibits a superior performance than that of g-MCMB at high charging rate.

The excellent rate performance of the prepared CTP-HC is ascribed to its unique structure which favors penetration the electrolyte and the transportation of electrons. Fig.4 schematically illustrated the lithium ion storage in CTP-HC and g-MCMB. First, the large specific surface area of the CTP-HC ensures a sufficient electrode/electrolyte interface for the absorption of lithium ions which promotes a rapid charge-transfer reaction. Second, the micropores in the CTP-HC can also act as reservoirs for the storage of lithium ions. Third, the porous structure of the CTP-HC can reduce the transport distance for the lithium ions from the bulk which enables the fast intercalation/deintercalation of the lithium ions. Moreover, the contacted graphite-like micro-crystallites ensure the fast and continuous transportation of electrons. As a combined result, the CTP-HC displays excellent electrochemical performance: high reversible capacity and initial coulombic efficiency, excellent rate performance and long cycling performance.

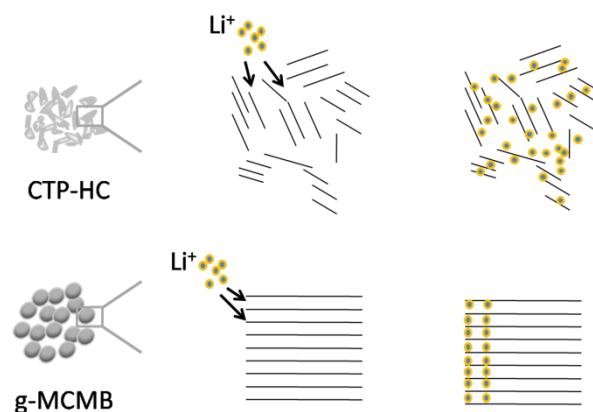


**Figure 4.** Schematic representation of lithium ion storage in CTP-HC and g-MCMB.

#### 4. CONCLUSIONS

Coal tar pitch-based hard carbon (CTP-HC) was prepared by a simple oxidation-carbonization method. Structural characterization indicates that the obtained hard carbon is poorly crystallized and contains some contacted graphite-like micro-crystallites. Because of high content of micropores and nanosized graphitic domains, the CTP-HC exhibits a high reversible capacity, an excellent rate performance and good cycle performance as the anode material in lithium ion batteries.

#### ACKNOWLEDGEMENTS

The work was financially supported by a Key Project of the Natural Science Foundation of Tianjin City (No. 09ZCKFGX02400) and National Nature Science Foundation of China (No. 51172160).

#### References

1. J.-M. Tarascon, M. Armand, *Nature*, 414 (2001) 359.
2. T. Horiba, T. Maeshima, T. Matsumura, M. Koseki, J. Arai, Y. Muranaka, *J. Power Sources*, 146 (2005) 107.
3. A. Funabiki, M. Inaba, Z. Ogumi, S.-I. Yuasa, J. Otsuji, A. Tasaka, *J. Electrochem. Soc.*, 145 (1998) 172.
4. Y.H. Liu, J.S. Xue, T. Zheng, J.R. Dahn, *Carbon*, 34 (1996) 193.
5. J.-C. Chang, Y.-F. Tzeng, J.-M. Chen, H.-T. Chiu, C.-Y. Lee, *Electrochim. Acta*, 54 (2009) 7066.
6. K.X. Wang, Z.L. Li, Y.G. Wang, H.M. Liu, J.S. Chen, J. Holmes, H. S. Zhou, *J.Mater.Chem.*, 20 (2010) 9748.
7. K. Tang, R.J. White, X.K. Mu, M.-M. Titirici, P.A. van Aken, J. Maier, *ChemSusChem*, 5 (2012) 400.
8. C. Kim, K.S. Yang, M. Kojima, K. Yoshida, Y.J. Kim, Y.A. Kim, M. Endo, *Adv. Funct. Mater.*, 16(2006) 2393.
9. I. Mochida, C.-H. Ku, Y. Korai, *Carbon*, 39 (2001) 399.
10. H. Fujimoto, K. Tokumitsu, A. Mabuchi, N. Chinnasamy, T. Kasuh, *J. Power Sources*, 195 (2010) 7452.
11. B.J. Yu, C.Y. Wang, M.M. Chen, J.M. Zheng, J.Qi, *Fuel Process. Technol.*, 104 (2012) 155.

12. A.C. Ferrari, J. Robertson, *Phys. Rev. B*, 61 (2000) 14095.
13. L. Zhang, H.D. Li, K.-T. Yue, S.-L. Zhang, X.H. Wu, J. Zi, Z.J. Shi, Z.N. Gu, *Phys. Rev. B*, 65 (2002) 073401.
14. L.J. Ci, H.W. Zhu, B.Q. Wei, C.L. Xu, J. Liang, D.H. Wu, *Mater. Lett.*, 43 (2000) 291.
15. R. Alcántara, G.F. Ortiz, P. Lavela, J.L. Tirado, R. Stoyanova, E. Zhecheva, *Chem. Mater.*, 18 (2006) 2293.
16. A. Gibaud, J.S. Xue, J.R. Dahn, *Carbon*, 34 (1996) 499.
17. Y.-P. Wu, C.-R. Wan, C.-Y. Jiang, S.-B. Fang, Y.-Y. Jiang, *Carbon*, 37 (1999) 1901.
18. L. Qie, W.-M. Chen, Z.-H. Wang, Q.-G. Shao, X. Li, L.-X. Yuan, X.-L. Hu, W.-X. Zhang, Y.-H. Huang, *Adv. Mater.*, 24 (2012) 2047.
19. V. Subramanian, H.W. Zhu, B.Q. Wei, *J. Phys. Chem. B*, 110 (2006) 7178.
20. S.S. Zhang, M.S. Ding, K. Xu, J. Allen, T.R. Jow, *Electrochem. Solid. ST.*, 4 (2001) 206.
21. C.W. Park, S.-H. Yoon, S.I. Lee, S.M. Oh, *Carbon*, 38 (2000) 995.